3D Bioprintable GelMA Ultrasound Responsive Scaffolds for Precise Micropatterning and Spatiotemporal Drug Release

Sabine Meurs, Mitra Aliabouzar

In recent years, there has been increasing interest in hydrogels as a platform for patient-specific treatments such as drug release. The term hydrogel refers to "networks of polymer chains that are sometimes found as colloidal gels in which water is the dispersion medium [1]". Possessing a variety of highly tunable mechanical properties, hydrogels can be synthesized using natural or synthetic materials to recapitulate the native biological environment. Natural materials tend to have inherent biocompatible properties such as the presentation of receptor-binding ligands and the ability to be proteolytically degraded and remodeled [2]. More generally, drug release and cell encapsulation, among others, are just some of the qualities that can be imparted into hydrogels. Despite these advantages, there is a stall in the development of highly mechanically tuned and user-defined hydrogels. To combat this, we have developed a composite hydrogel, termed an acoustically responsive scaffold (ARS), that enables spatiotemporally controlled drug delivery using focused ultrasound [3][4]. An ARS consists of a phase-shift emulsion (PSE) embedded within a hydrogel matrix. Upon exposure to ultrasound, the emulsion undergoes acoustic droplet vaporization (ADV), thereby releasing payloads initially encapsulated within the emulsion. Similar to conventional hydrogels, ARSs have previously been polymerized using bulk polymerization techniques. There are inherent limitations with this approach as it doesn't enable precise spatial patterning of the PSE within the ARSs. Firstly this is to owed to the form factor of the ARS being dictated by the shape of the container that holds the solution during cross-linking. Second, the ability to generate complex patterns of emulsions within an ARS is very limited.

A potential solution to generate ARSs with complex form factors and intricate patterns of emulsions is extrusion-based 3D printing, as it is a type of additive manufacturing that enables layer-by-layer fabrication of an ARS based on user-defined, computer-aided design. Using 3D bioprinting allows limitations with engineered tissue constructs to be overcome. One of the principal challenges for engineered tissue constructs is ensuring the construct integrates quickly within the body. Conventional hydrogels inherently contain pores that are much smaller than the diameter of a cell. Thus, for a cell to infiltrate a hydrogel, the cell must enzymatically degrade the hydrogel surrounding it, which can be a slow process. One widely used approach to increase the rate at which a cell can traverse a hydrogel is to create macropores. These macropores, which are on the order of 50-200 microns in diameter, enable cells to rapidly migrate within a scaffold. A commonly used method for creating macropores within a hydrogel is a technique called porogen leaching, where salt crystals are embedded within the scaffold and then subsequently dissolved. However, porogen leaching cannot be done in situ and the ability to spatially control the location and arrangement of the generated pores is very limited. Another challenge for engineered tissue constructs is modulated and temporally controlled drug dosage and delivery sequence to recapitulate natural biological processes.

This study proposes solutions to both of these challenges by presenting a method for coupling ADV and ARSs with highly-defined, complex structures to enable greater spatiotemporal control of both biological and biophysical cues. One of the methods explored in this study is generating ADV-induced macropores in ARSs through ultrasound-induced microjetting. Microjetting occurs when oscillating bubbles, generated by ADV, collapse near a boundary. We are able to establish boundaries within the hydrogel construct by alternating layers of different biomaterials such as fibrin, hyaluronic acid, and alginate. The technique developed would allow macropores to be generated in a spatiotemporally controlled manner for ARSs that are implanted in situ. For the second part of the study, to modulate drug release in an on-demand manner, ARSs containing two different payload-carrying emulsions. This was done using gelatin methacrylate (GelMA), a gelatin-based biomaterial used for tissue engineering. Ultrasound at two different frequencies was used to allow sequential release.

Materials and Methods

Microfluidic production of PSEs

As discussed in previous publications, a microfluidic technique was used to generate PSEs with a water (W1)-in-perfluorocarbon-in-water (W2) structure (Figure 1, right). They were manufactured via the use of a microfluidic chip (Cat# 3200146, junction: 14 μm × 17 μm, Dolomite, Royston, United Kingdom)[5] (Figure 1, left). Perfluorohexane (C6F14, CAS# 355-42-0, Strem Chemicals) or perfluorooctane (C8F18, CAS# 307–34–6, Sigma-Aldrich, St. Louis, MO, USA) were used as perfluorocarbon liquid cores. Two fluorescently-labeled dextrans were used to label the PSEs in this study: Alexa Fluor 488-labeled dextran (AF488, 10 kDa, Life Technologies, Grand Island, NY, USA) and Alexa Fluor 555-labeled dextran (AF555, 10 kDa, Life Technologies).

To produce monodispersed, micron-sized PSEs with different average diameters (Ø), the primary emulsion and W2 phase, which was 50 mg/mL Pluronic F68 (CAS# 9003-11-6, Sigma-Aldrich) in PBS, were pumped at two different flow rate combinations: i) inner and outer channels at 1 μL/min and 10 μL/min, respectively and ii) inner and outer channels at 0.5 μL/min and 2.5 μL/min, respectively. The emulsions were characterized using a Coulter Counter (Multisizer 4, Beckman Coulter, Brea, CA, USA) with a 30 μm aperture tube [6].

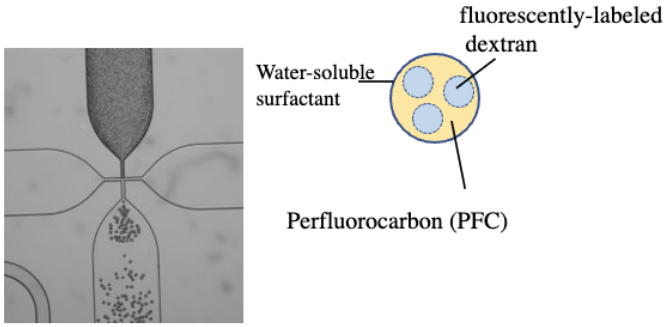


Figure 1. Microfluidic Production(left) of Phase-shift droplets (right)

Preparation and photopolymerization of acoustically-responsive bioinks

In this study, we used an extrusion-based method for 3D bioprinting of ARSs. Monodispersed PSEs were loaded into previously optimized, functional bioinks (i.e., hydrogel precursors) consisting of fibrin and/or cellulose nanofibrils or GelMA to build off of previous success with fibrin, hyaluronic acid, and/or alginate ARSs (Figure 2).

Acoustically-responsive GelMA bioinks were prepared by first adding 2-hydroxy-4'-(2-hydroxyethoxy)-2-methylpropiophenone powder (CAS#106797-53-9, Sigma-Aldrich) to PBS at 60℃ under stirring to create a 0.5% w/v concentration. Then the solution was cooled to 37℃ and gelatin methacryloyl powder (gelatin methacryloyl, Sigma-Aldrich) was added to create a 10% w/v concentration. Acoustically-responsive alginate bioinks for creating macropores via asymmetrical collapse of ADV bubbles were prepared by adding sodium alginate powder (alginic acid sodium salt, CAS# 9005-38-3, Sigma-Aldrich) to deionized (DI) water at 10% (w/v) and dissolving it overnight. A 20 mg/mL fibrin, 30 mg/mL alginate, and 4.5 mg/mL hyaluronic acid (HA) bioink was prepared by separately mixing stock solutions of fibrinogen, alginate, and HA at a 1:1 volume ratio. In this study, acoustically responsive bioinks containing PSEs were prepared by adding a 1% w/v concentration of perfluorohexane or perfluorooctane PSEs to the bioink. In all cases following preparation, bioinks were placed into 3 mL syringes (Cellink) and kept at 4 °C until use.

Fibrin-Alg-HA ARSs were spray crosslinked with 50 U/mLbovine thrombin (Thrombin-JMI, King Pharmaceuticals, Bristol, TN, USA) and 50 mg/mL calcium chloride (Sigma Aldrich) on a layer-by-layer basis during printing. After printing, Fibrin-Alg-HA ARSs were immersed in a 20 U/mL thrombin- 10 mg/mL crosslinking solution for half-hour polymerization. GelMA ARSs were also crosslinked on a layer-by-layer basis using the Cellink built-in photocuring 365 nm module at a distance of 4 cm for 6o seconds per layer. After printing GelMA ARSs were placed under the UV 365 nm photocuring module for 10 minutes.

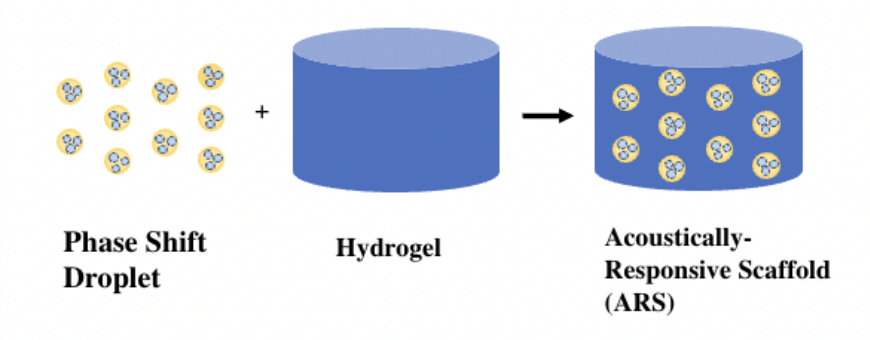


Figure 2. Schematic of acoustically responsive scaffold (ARS)

Bioprinting setup and process control for acoustically-responsive bioinks

CAD models were created in SolidWorks (Dassault Systémes, Waltham, MA, USA) and then transferred as STL files to the open-source software, Slic3r (https://slic3r.org/). Slic3r then enabled the generation of a G-code that could be uploaded to the 3D bioprinter pictured below in Figure 3(Bio X, Cellink, USA). Samples with GelMA bioink were printed using 3 mL temperature-controlled pneumatic printheads. A 25-gauge needle, with an inner diameter (D) of 250 μm and length (L) of 12.7 mm, was used for all GelMA ARSs. A 27-gauge needle, with an internal diameter (D) of 200 μm and length (L) of 6.35 mm, was used for the microjetting prints.

Ultrasound Exposure and Acoustic Droplet Vaporization

ADV was generated using a focused ultrasound transducer at 2.5 MHz and peak rarefactional pressures of 4-6 MPa (Figure 3). All the ADV experiments were conducted in a water tank. Exposures were monitored in real-time using an oscilloscope.

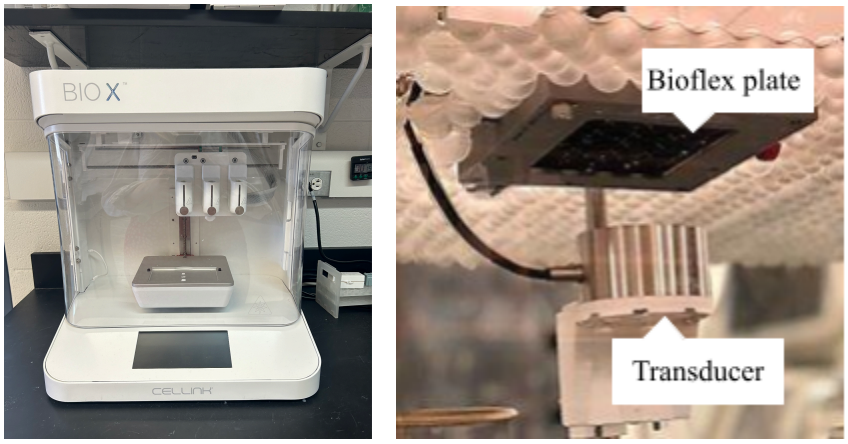


Figure 3. Cellink Bioprinter (left) and Ultrasound Setup (right)

Optical imaging and analyses

Effects of ADV-generated bubble dynamics in bilayer ARSs were imaged using confocal and epifluorescence microscopy (Eclipse TiE, Nikon, Melville, NY, USA) and acquisition software (MetaMorph, Molecular Devices, San Jose, CA, USA).

Results

Spatial Patterning and Complex Geometries

Bioprinting facilitates the fabrication of layered ARSs with varying mechanical properties as well as complex geometries. One of the benefits provided by bioprinting is the potential for patient-specific patterning as can be seen by the vascular print in Figure 4 below. Other benefits include the ability to print multiple payloads within a singular layer in lieu of stacking individual layers of payloads as is often seen in conventional hydrogel production methods. Said layer-by-layer printing enables the control of the acoustic response of ADV-induced bubbles, as well as cell integration and patterning.

CAD Model

3D Bioprinted

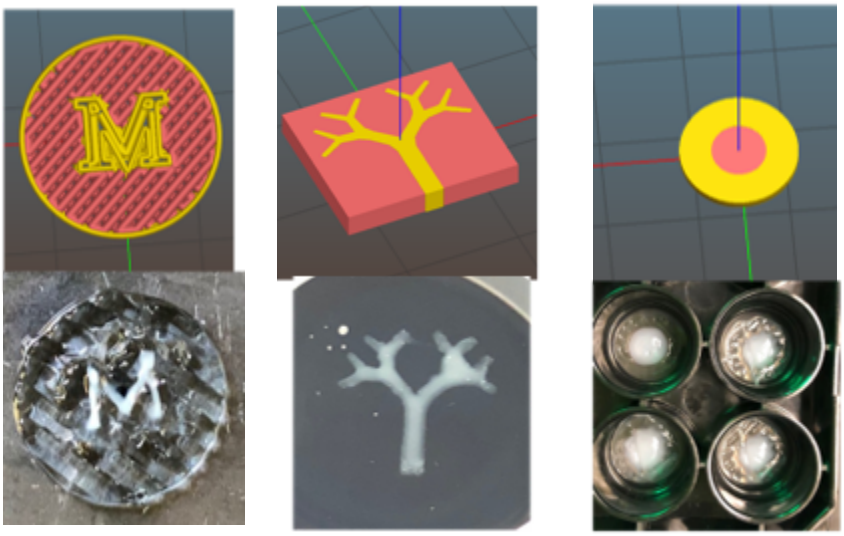


Figure 4. 3D Printed complex geometries

Macropore Formation

Varying the elastic modulus of the hydrogel serves to modulate bubble kinematics as well as release. In conventional monolayers, as in a hydrogel with a uniform elastic modulus, spherical bubbles are formed that grow significantly with time as they are gas bubbles by the principle of passive diffusion. A visual representation of bubbles in a conventional monolayer can be seen on

the left in Figure 5. This is in comparison with the image on the right, where the bubbles can be seen collapsing asymmetrically near a rigid alginate layer. The contrast between the two images points towards the impact of spatiotemporally controlling dynamics through bioprinting. As can be seen in these images, visible pitting and indents within the rigid alginate layer. A maximum of 35 µm deep tunneling was achieved using the 2.5 MHz frequency transducer [6].

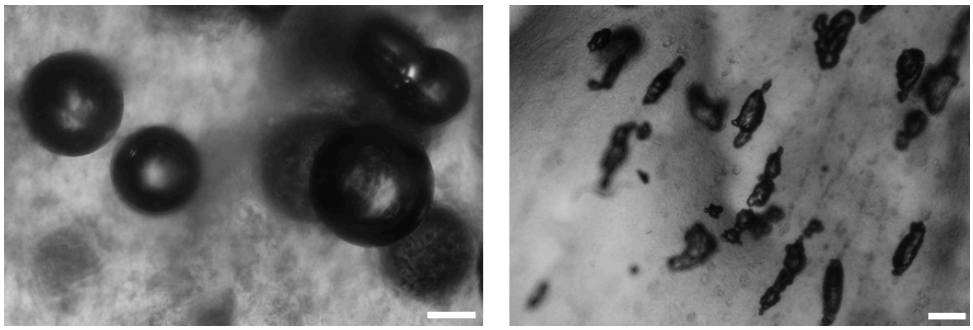


Figure 5. Conventional monolayer bubble formation (left) and macropore formation (right)

The formation of macropores over passively diffusing bubbles is further validated by quantifying the area of ADV-generated features in a monolayer construct vs a bilayer with varying mechanical properties (Figure 6). Additionally in a time-dependent study comparing said areas again in Figure 6, it can be seen that the features generated in a bilayer with a rigid layer do not grow over time which points to their fluid-filled nature. In contrast, the bubble area can be seen to grow significantly in the uniform construct. Together these point to existence of macropores formed by the asymmetrical collapse of ADV-formed bubbles against the rigid alginate layer.

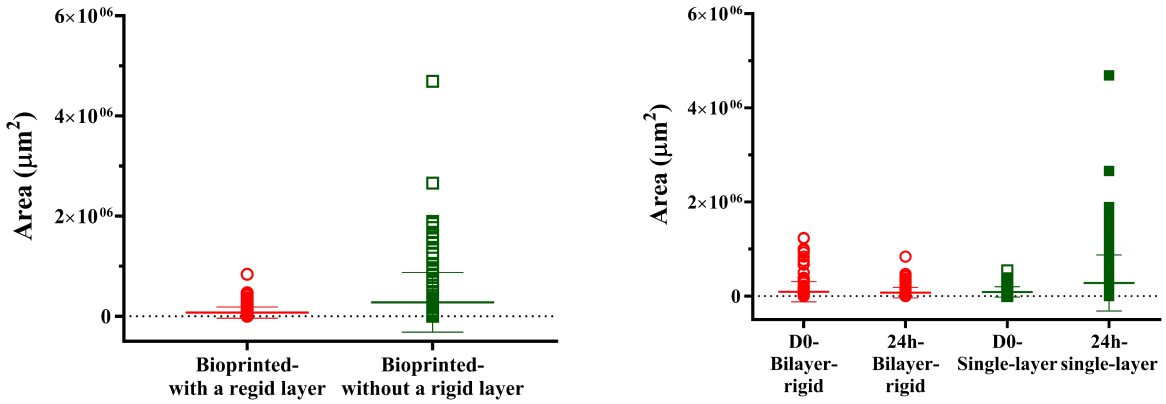


Figure 6. Comparing the area of ADV-generated features in monolayer vs. bilayer immediately post US (left) and over time (right)

Furthermore, the fluorescent images below in Figure 7 show how the integration of bioprinting

with ADV can be seen to enable control of bubble dynamics and in return release kinetics due to bubble collapse and subsequent macropore formation.

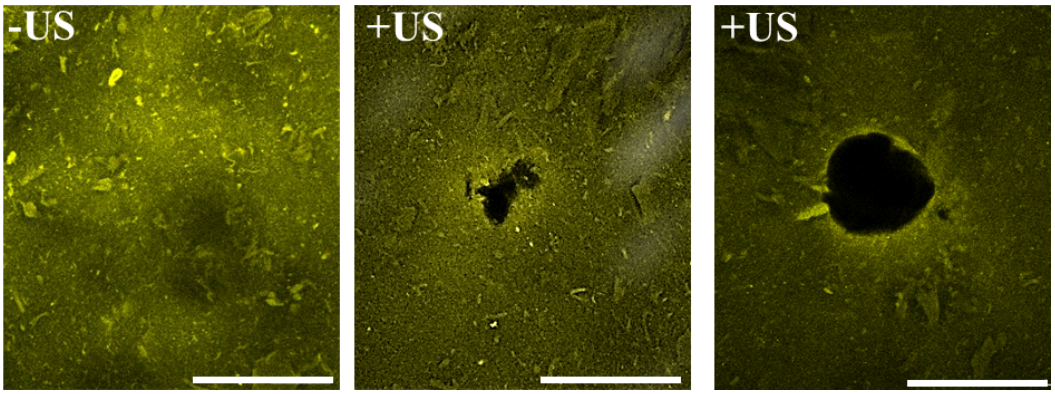


Figure 7. Fluorescent images of spatially controlled ADV

Single and Dual Sequential Payload Release in GelMA ARSs

Before printing dual-release hydrogels, which are hydrogels with two different PSEs, single-release GelMA ARSs were printed to reaffirm previous studies that used fibrin, alginate, and other materials with PSEs. As can be seen in Figure 8 below, a monolayer of 10% GelMA ARS with perfluorohexane fluorescently labeled with 488 was printed. Said monolayer ARS was printed to establish the single release of perfluorohexane in an on-demand manner. Figure 8 displays the formation of ADV-induced bubbles following ultrasound exposure of the ARS. The single-release GelMA ARSs serve as a benchmark for the dual sequential payload release, as well as help establish the basic printing and ultrasound exposure parameters. Studies optimizing the hydrogels' 10% GelMA composition, the UV crosslinking duration of 60 seconds, the 30℃ printhead temperature, the 15℃ print bed temperature, the 12 kPa printing pressure, and the 10 mm/s printhead speed were conducted via printing the single monolayer GelMA ARSs.

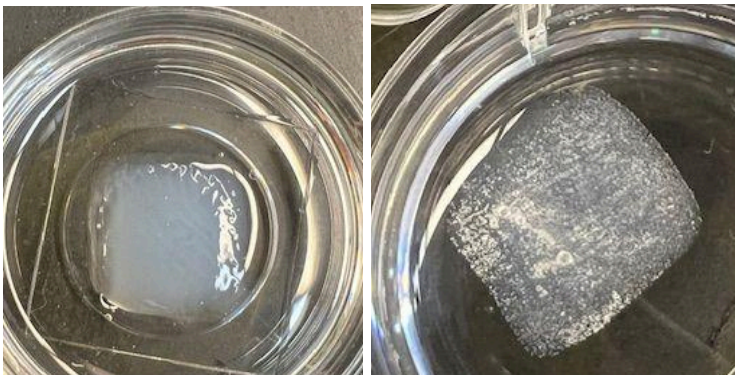


Figure 8. Single C6 Payload Release in 14mm x 14mm x 1 mm 10% GelMA ARS before (left) and after ultrasound exposure (right)

Moving on to a concentric square model as can be seen below in Figure 9, an embedded square system with a dual payload release was bioprinted to prove temporal control. As can be seen in Figure 9A, a larger square measuring 14 mm x 14 mm with a smaller square measuring 7 mm x 7 mm was printed. Then in Figure 9B, the confocal image of the ultrasound-exposed GelMA ARS can be seen, and minimal mixing and precise spatial patterning is shown (Figure 9C, 9D). Furthermore, as can be seen in Figure 10, one payload was designed to be ultrasound released on Day 0, while the second payload was released on Day 3.

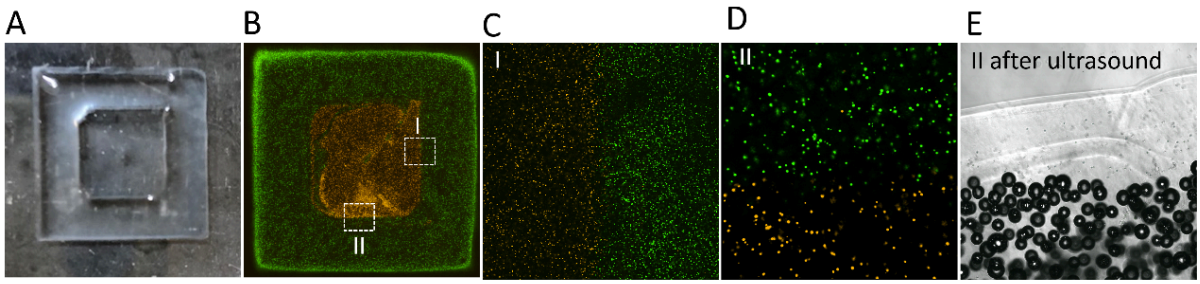


Figure 9. (A) A picture of a 3D-bioprinted ARS with two concentric square patterns (14 mm × 14 mm and 7 mm × 7 mm). (B) 3D-bioprinted ARS after 1st payload release. (C) A confocal image of the 3D-bioprinted, GelMa-based ARS containing two fluorescently-labeled droplets shown in yellow (C6F14) and green (C8F18). Enlarged images in (D) and (E) demonstrate precise micropatterning and minimal mixing at the interfaces.

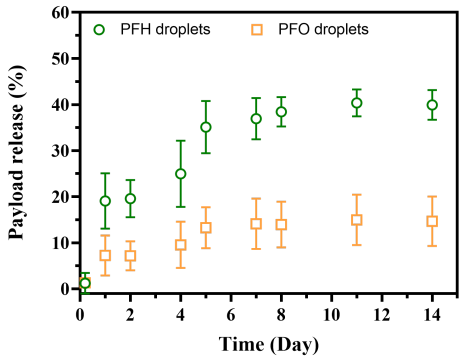


Figure 10. Dual Sequential Payload Release of PFO and PFH in 10% GelMA

Embedded Discs Prints

To further validate the spacial micropatterning achievable using the 3D bioprinter, 17 mm discs were printed with two 4 mm discs in the center spaced apart from each other. Only the inner

discs contained fluorescently labeled perfluorohexane PSEs, and this spatial patterning was maintained following ultrasound exposure as can be seen below in Figure 11.

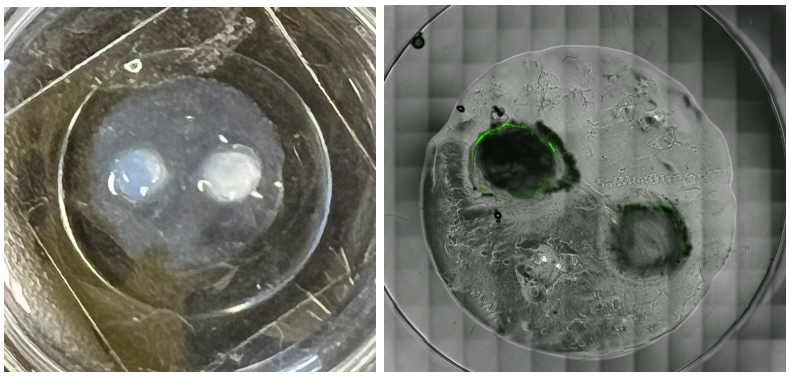


Figure 11. Perfluorohexane-embedded GelMA ARS disc before (left) and after ultrasound exposure (after)

Discussion

As of yet, there has not been a method for drug release combining the use of ultrasound-modulated drug release and a 3D bioprinted scaffold so this study presents a new method that has the potential for widespread use in therapeutic applications. Currently, many hydrogels and drug delivery scaffolds use diffusion as their primary control on drug release, while in contrast, this method proposes complete non-invasive control of a drug in a patient over time via controlled ultrasound. Other factors that contribute to this non-invasive control are defined by the bioprinting parameters and material characteristics as can be seen by the macropore formation aim elaborated upon in this study. Notably, 3D bioprinting allows for the production of spatially defined and controlled ARSs that can be patient as well as drug specific. On the other hand, payload release kinematics and macropore formation can be modulated by varying the elastic modulus of layers within the ARS as well as ultrasound parameters.

Acknowledgments

I would like to thank Mitra Aliabouzar and Mario Fabiilli for their mentorship and support throughout this project and my research with them over the last four years.

References

[1] Ahmed E. M. (2015). Hydrogel: Preparation, characterization, and applications: A review. Journal of advanced research, 6(2), 105–121. https://doi.org/10.1016/j.jare.2013.07.006

[2] Lutolf, M. P., & Hubbell, J. A. (2005). Synthetic biomaterials as instructive extracellular microenvironments for morphogenesis in tissue engineering. Nature biotechnology, 23(1), 47–55. https://doi.org/10.1038/nbt1055

[3] Moncion, A., Lin, M., O'Neill, E. G., Franceschi, R. T., Kripfgans, O. D., Putnam, A. J., & Fabiilli, M. L. (2017). Controlled release of basic fibroblast growth factor for angiogenesis using acoustically-responsive scaffolds. Biomaterials, 140, 26-36. doi:10.1016/j.biomaterials.2017.06.012

[4] Dong, X., Lu, X., Kingston, K., Brewer, E., Juliar, B. A., Kripfgans, O. D., . . . Fabiilli, M. L. (2019). Controlled delivery of basic fibroblast growth factor (bfgf) using acoustic droplet

vaporization stimulates endothelial network formation. Acta Biomaterialia, 97, 409-419. doi:10.1016/j.actbio.2019.08.016

[5] Aliabouzar M, Lu X, Kripfgans OD, Fowlkes JB, Fabiilli ML, Acoustic droplet vaporization in acoustically responsive scaffolds: effects of frequency of excitation, volume fraction and threshold determination method, Ultrasound Med. Biol 45 (12) (2019) 3246–3260. [PMC free article] [PubMed] [Google Scholar]

[6] Aliabouzar, M., Ley, A. W. Y., Meurs, S., Putnam, A. J., Baker, B. M., Kripfgans, O. D., Fowlkes, J. B., & Fabiilli, M. L. (2022). Micropatterning of acoustic droplet vaporization in acoustically-responsive scaffolds using extrusion-based bioprinting. Bioprinting (Amsterdam, Netherlands), 25, e00188. https://doi.org/10.1016/j.bprint.2021.e00188